Analysis of Numerical Dispersion in the High-Order 2-D WLP-FDTD Method

Wei-Jun Chen[1, *], Jun Quan[2], and Shi-Yu Long[1]

Abstract—A theoretical analysis of numerical dispersion in the high-order finite-difference time-domain (FDTD) method with weighted Laguerre polynomials (WLPs) is proposed in this paper. According to the numerical dispersion relation for the two-dimensional (2-D) case, the numerical phase velocities relevant to the direction of wave propagation, grid discretization and time-scale factor are obtained. For a fixed relative error of the numerical phase velocity, the suitable sampling point density and time-scale factor can be determined. Compared with the low-order WLP-FDTD, the high-order one shows its good dispersion characteristics while a low sampling density is used. Three numerical examples are included to validate the effectiveness of the high-order scheme.

1. INTRODUCTION

The finite-difference time-domain (FDTD) method is a very popular time-domain method for solving electromagnetic problems, but its time step is constrained by the Courant-Friedrich-Levy (CFL) stability condition [1]. To overcome this limitation, an unconditionally stable FDTD method, which combines weighted Laguerre polynomials (WLPs) as the basis function with Galerkin's testing procedure, was proposed by Chung et al. [2]. For some problems with fine structures, this method shows much better efficiency than the conventional FDTD method.

Generally, WLP-FDTD results in a huge sparse matrix equation, which is challenging to solve. In [3–6], the factorization-splitting techniques were proposed to divide the huge matrix into small ones corresponding to different electromagnetic components. Based on the solution of the Schur complement system, a domain decomposition scheme is implemented in WLP-FDTD to improve the efficiency [7]. To reduce the number of unknowns in the huge matrix, scaling functions [8] and mixed-order scheme [9] are introduced into WLP-FDTD to decrease the sampling density in space domain, respectively. Thus, the produced sparse matrix with a much smaller number of unknowns leads to a more efficient solution of WLP-FDTD.

For the fourth-order WLP-FDTD method, an analysis of numerical dispersion for the two-dimensional (2-D) case is presented in this paper. Besides the direction of wave propagation and grid discretization, the time-scale factor s is necessarily involved and influences the dispersion errors to a great degree. From its numerical dispersion relation, small relative errors of the numerical phase velocity can be obtained while the low sampling density is used. Three numerical examples are tested to show the necessity of numerical dispersion analysis in the high-order scheme.

2. NUMERICAL DISPERSION ANALYSIS

The time-domain Maxwell's equations for a 2-D TEz wave propagating in free space can be written as

$$\varepsilon_0 \frac{\partial E_x \mid_{x,y,t}}{\partial t} = \frac{\partial H_z \mid_{x,y,t}}{\partial y}, \tag{1a}$$

$$\varepsilon_0 \frac{\partial E_y \mid_{x,y,t}}{\partial t} = -\frac{\partial H_z \mid_{x,y,t}}{\partial x}, \tag{1b}$$

$$\mu_0 \frac{\partial H_z \mid_{x,y,t}}{\partial t} = \frac{\partial E_x \mid_{x,y,t}}{\partial y} - \frac{\partial E_y \mid_{x,y,t}}{\partial x}, \tag{1c}$$

where ε_0 and μ_0 are the electric permittivity and magnetic permeability of free space, respectively. With reference to [2], the 2-D implicit formulation for WLP-FDTD can be given by introducing the Laguerre basis functions and Galerkin's testing procedure

$$E_x^p \mid_{x,y} = \frac{2}{s\varepsilon_0} \frac{\partial H_z^p \mid_{x,y}}{\partial y} - 2 \sum_{\substack{q=0, \\ p>0}}^{p-1} E_x^q \mid_{x,y}, \tag{2a}$$

$$E_y^p \mid_{x,y} = -\frac{2}{s\varepsilon_0} \frac{\partial H_z^p \mid_{x,y}}{\partial x} - 2 \sum_{\substack{q=0, \\ p>0}}^{p-1} E_y^q \mid_{x,y}, \tag{2b}$$

$$H_z^p \mid_{x,y} = \frac{2}{s\mu_0} \frac{\partial E_x^p \mid_{x,y}}{\partial y} - \frac{2}{s\mu_0} \frac{\partial E_y^p \mid_{x,y}}{\partial x} - 2 \sum_{\substack{q=0, \\ p>0}}^{p-1} H_z^q \mid_{x,y}, \tag{2c}$$

where s is the time-scale factor and p is the order of Laguerre functions. For a monochromatic wave, E_x^p, E_y^p and H_z^p are expanded into a discrete set of Fourier modes as follows [6, 10]:

$$\left\{ E_x^p \mid_{i,j}, E_y^p \mid_{i,j}, H_z^p \mid_{i,j} \right\} = \left\{ E_x^p, E_y^p, H_z^p \right\} e^{j_0(ik\Delta x \cos\varphi + jk\Delta y \sin\varphi)}, \tag{3}$$

where (i, j) denotes the spatial index of a field component, Δx and Δy are the space steps along the x- and y-axes, $j_0 = \sqrt{-1}$, k is the wavenumber, and φ is the angle between the propagation direction and x-axis. The fourth-order central-difference formula for staggered grids can be written as [11]

$$\frac{df(x)}{dx} = \frac{9}{8} \frac{f(x+0.5\Delta x) - f(x-0.5\Delta x)}{\Delta x} - \frac{1}{24} \frac{f(x+1.5\Delta x) - f(x-1.5\Delta x)}{\Delta x}. \tag{4}$$

Inserting (3) and (4) into (2), we get

$$E_x^p - \frac{H_z^p \left[27 \left(e^{j_0 b} - e^{-j_0 b} \right) - \left(e^{j_0 3b} - e^{-j_0 3b} \right) \right]}{12 s\varepsilon_0 \Delta y} = -2 \sum_{\substack{q=0, \\ p>0}}^{p-1} E_x^q, \tag{5a}$$

$$E_y^p + \frac{H_z^p \left[27 \left(e^{j_0 a} - e^{-j_0 a} \right) - \left(e^{j_0 3a} - e^{-j_0 3a} \right) \right]}{12 s\varepsilon_0 \Delta x} = -2 \sum_{\substack{q=0, \\ p>0}}^{p-1} E_y^q, \tag{5b}$$

$$\frac{27 \left(e^{j_0 b} - e^{-j_0 b} \right) - \left(e^{j_0 3b} - e^{-j_0 3b} \right)}{-12 s\mu_0 \Delta y} E_x^p + \frac{27 \left(e^{j_0 a} - e^{-j_0 a} \right) - \left(e^{j_0 3a} - e^{-j_0 3a} \right)}{12 s\mu_0 \Delta x} E_y^p + H_z^p = -2 \sum_{\substack{q=0, \\ p>0}}^{p-1} H_z^q \tag{5c}$$

where $a = 0.5k\Delta x \cos\varphi$ and $b = 0.5k\Delta y \sin\varphi$. Using Euler's formula, (5) can be written in a matrix form as

$$\mathbf{A E}^p = \sum_{q=0, p>0}^{p-1} \mathbf{E}^q, \tag{6}$$

where $\mathbf{E}^p = [E_x^p, E_y^p, H_z^p]^T$, $\mathbf{E}^q = [E_x^q, E_y^q, H_z^q]^T$ and

$$
\mathbf{A} = \begin{bmatrix} -\dfrac{1}{2} & 0 & j_0\dfrac{27\sin b - \sin(3b)}{12s\varepsilon_0\Delta y} \\[2ex] 0 & -\dfrac{1}{2} & j_0\dfrac{27\sin a - \sin(3a)}{-12s\varepsilon_0\Delta x} \\[2ex] j_0\dfrac{27\sin b - \sin(3b)}{12s\mu_0\Delta y} & j_0\dfrac{27\sin a - \sin(3a)}{-12s\mu_0\Delta x_0} & -\dfrac{1}{2} \end{bmatrix}
$$

While $p = 0, 1, \ldots, N-1, N$, where N is the largest order of the Laguerre function, we have

$$
\begin{bmatrix} \mathbf{A} & 0 & 0 & \ldots & 0 & 0 & 0 \\ -\mathbf{I} & \mathbf{A} & 0 & \ldots & 0 & 0 & 0 \\ -\mathbf{I} & -\mathbf{I} & \mathbf{A} & \ldots & 0 & 0 & 0 \\ \vdots & \vdots & \vdots & \ddots & \vdots & \vdots & \vdots \\ -\mathbf{I} & -\mathbf{I} & & \ldots & -\mathbf{I} & \mathbf{A} & 0 \\ -\mathbf{I} & -\mathbf{I} & & \ldots & -\mathbf{I} & -\mathbf{I} & \mathbf{A} \end{bmatrix} \begin{bmatrix} \mathbf{E}^0 \\ \mathbf{E}^1 \\ \mathbf{E}^2 \\ \vdots \\ \mathbf{E}^{N-1} \\ \mathbf{E}^N \end{bmatrix} = 0 \tag{7}
$$

where I is a 3×3 identity matrix. For a nontrivial solution of homogeneous Equation (7), the determinant of its coefficient matrix should be zero, thus leading to $|A|^{N+1} = 0$. Consequently, it can be derived

$$
\frac{729\sin^2 b}{\Delta y^2} + \frac{\sin^2(3b)}{\Delta y^2} - \frac{54\sin b\sin(3b)}{\Delta y^2} + \frac{729\sin^2 a}{\Delta x^2} + \frac{\sin^2(3a)}{\Delta x^2} - \frac{54\sin a\sin(3a)}{\Delta x^2} = -\frac{144s^2\varepsilon_0\mu_0}{4}. \tag{8}
$$

When $\Delta x = \Delta y \to 0$ in (8), the theoretical solution of the time-scale factor can be expressed as

$$
s_0 = |\text{Im}(s)| = \frac{2k}{\sqrt{\varepsilon_0\mu_0}} = 4\pi f_0, \tag{9}
$$

where f_0 is the operating frequency. It can be seen from (8) that the numerical dispersion of high-order WLP-FDTD relates to the propagation direction, sampling density in space domain and time-scale factor. The relative error of the numerical phase velocity is:

$$
\delta_r = \left| \frac{\nu_p - c}{c} \right| = \left| \frac{1}{24\pi\delta}\frac{s_0}{s}\sqrt{\begin{bmatrix} 729\sin^2(\pi\delta\sin\varphi) + \sin^2(3\pi\delta\sin\varphi) \\ -54\sin(\pi\delta\sin\varphi)\sin(3\pi\delta\sin\varphi)+ \\ 729\sin^2(\pi\delta\cos\varphi) + \sin^2(3\pi\delta\cos\varphi) \\ -54\sin(\pi\delta\cos\varphi)\sin(3\pi\delta\cos\varphi) \end{bmatrix}} - 1 \right|, \tag{10}
$$

where v_p is the numerical phase velocity, $c = 1/\sqrt{\varepsilon_0\mu_0}$ is the speed of light in free space, $\delta = \Delta x/\lambda_0 = \Delta y/\lambda_0$ and λ_0 is the operating wavelength.

Figure 1 plots two regions that denote two different intended error ranges, $\delta_r \leq 0.005$ and $0.005 < \delta_r \leq 0.01$. Here, the errors are the maximum ones for $\varphi \in [0°, 90°]$ in (10). If the value of an intended error is given, it is easy to determine the suitable combinations of s and δ.

Figure 2(a) plots the curves which illustrate the variation of v_p with propagation angle φ. Here, three different sampling densities with three different values of s/s_0 are examined. For comparison, the variation in the low-order method is also calculated in Figure 2(b). v_p is dependent upon the direction of wave propagation and it is maximum for waves propagating obliquely with the grid ($\varphi = 45°$). To obtain acceptable numerical dispersion errors, fewer grid cells per wavelength are required than those in low-order WLP-FDTD. It is noteworthy from Figure 2 that the value of the time-scale factor s also determines the numerical error. When $s_0/s = 1$, v_p is much closer to the speed of light c than the other cases.

3. NUMERICAL RESULTS

As the first example, the first two cutoff frequencies of a 2-D air-filled rectangular waveguide ($1.2\,\text{m} \times 0.6\,\text{m}$) are calculated with high-order WLP-FDTD. A sinusoidally modulated Gaussian pulse

Table 1. Comparison between different time-scale factors.

	TE$_{10}$		TE$_{20}$	
	Solution (MHz)	Error (%)	Solution (MHz)	Error (%)
Analytic	124.94	-	249.89	-
$0.98s_0$	125.06	0.096	248.98	0.37
$0.99s_0$	125.01	0.054	248.98	0.37
s_0	125.01	0.054	249.13	0.30
$1.01s_0$	124.96	0.013	249.05	0.33
$1.02s_0$	125.03	0.075	249.03	0.34

is used as the incident electric current profile:

$$J_x(t) = \exp\left[-\left(\frac{t - T_c}{T_d}\right)^2\right] \sin\left[2\pi f_c \left(t - T_c\right)\right], \tag{11}$$

where $T_d = 1/(2f_c)$, $T_c = 6T_d$ and $f_c = 0.2\,\text{GHz}$. And we choose the time duration $T_f = 160\,\text{ns}$. This duration is chosen in such a way that the waveforms of interest have practically decayed to zero [2]. Assuming the maximum operating frequency $f_{\max} = 520\,\text{MHz}$, we can obtain $s = 6.5345 \times 10^9$ with (9) and $N = 272$ from [10]. In this example, uniform square cells with $\Delta x = \Delta y = 0.1\,\text{m}$ (about six cells per λ, where λ is the wavelength corresponding to $f_{\max}$) are used to divide the 2-D space domain.

By performing the fast Fourier transform (FFT) to the time-domain data from the high-order WLP-FDTD with different time-scale factor s, we can obtain the first two cutoff frequencies and the relative error, results as shown in Table 1. From Table 1, it is seen that the relative errors are all very small ($< 0.1\%$) for TE$_{10}$ mode. And the error is the smallest while the time-scale factor s is chosen as the theoretical solution s_0 for TE$_{20}$ mode.

As the second example, the cutoff frequencies of the first two modes in a 2-D partially loaded rectangular waveguide, shown in Figure 3, are calculated. Since the geometry is uniform in the y direction, the TE$_{10}$ and TE$_{20}$ modes have no y dependence [12]. The same modulated Gaussian pulse and parameters as the first example are used.

Table 2 shows the computational efforts and results with the high-order and low-order WLP-FDTD methods for different grid divisions. Considering the low-order WLP-FDTD method with the fine mesh (120×60) as the benchmark, the high-order scheme shows its accurate results when occupying smaller meshing size and less CPU time.

The third example is to calculate the reflected signal power in a 2-D parallel plate waveguide with a thin dielectric interface, shown in Figure 4. The same modulated Gaussian pulse as (11) is used as x-direction input current profile with $f_c = 0.4\,\text{GHz}$. And we choose the time duration $T_f = 80\,\text{ns}$.
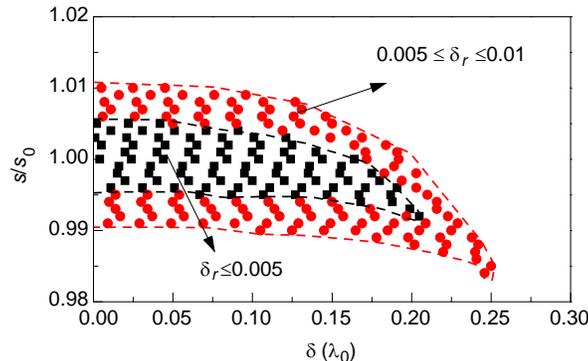
Figure 1. Regions to determine s and δ for an intended fixed error.
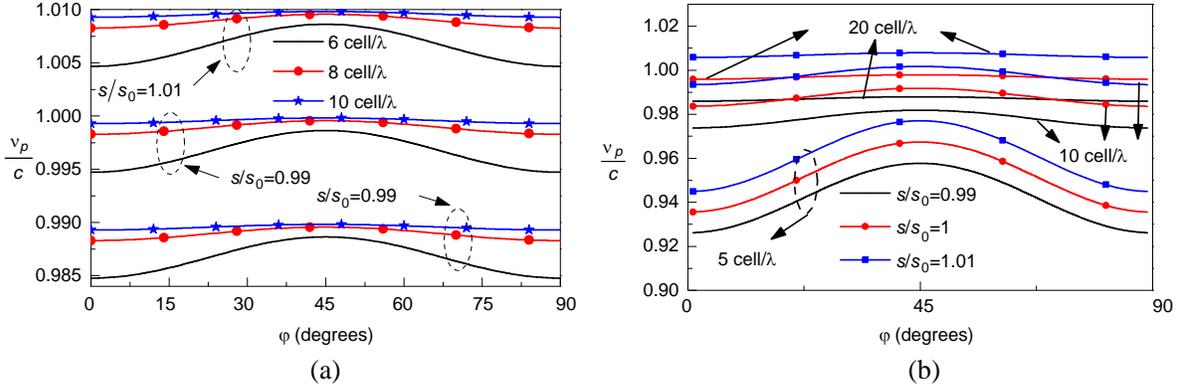
Figure 2. Variation of numerical phase velocity with the propagation angle, sampling density and time-scale factor in (a) high-order and (b) low-order method.

Table 2. Comprison between high- and low-order schemes.

Method	Meshing size	Time (s)	TE$_{10}$ mode		TE$_{20}$ mode	
			Fre. (MHz)	Difference (%)	Fre. (MHz)	Difference (%)
High-order scheme	30×15	4.6	117.456	0.22	190.440	0.10
	40×20	10.2	117.600	0.10	191.088	0.09
Low-order scheme	40×20	5.1	117.480	0.20	189.528	0.90
	60×40	12.1	117.600	0.10	190.244	0.53
	120×60	69.5	117.720	-	191.256	-
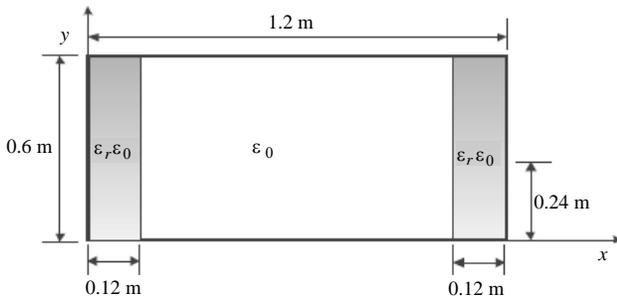
Figure 3. Cross-section of a 2-D waveguide loaded with a dielectric block of $\varepsilon_r = 9$.
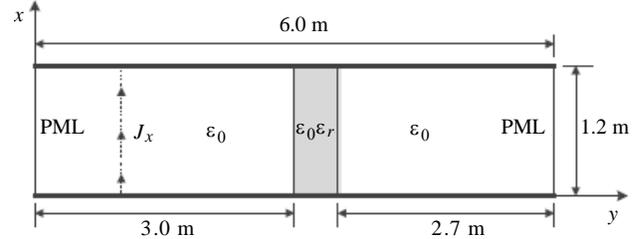
Figure 4. 2-D parallel plate waveguide with a thin dielectric interface of $\varepsilon_r = 9$.

Assuming the maximum operating frequency $f_{\max} = 1\,\text{GHz}$, we can obtain $s = 1.2566 \times 10^{10}$ with (9) and $N = 261$ from [10]. A perfectly matched layer (PML) with 2nd-order central-difference as the absorbing boundary condition is used to truncate the open areas [9]. In this example, the PML includes '8 layers with quadratic polynomial increase of conductivity of 0.1% theoretical reflection coefficients at normal incidence.

From the calculated temporal electric fields, the reflected signal powers are obtained through discrete Fourier transform (DFT). Figure 5 shows that the reflected signal powers from the high-order and low-order WLP-FDTDs with different grid discretization. Table 3 shows the requirement of CPU time and memory. Considering the low-order method with the grid discretization of $15\,\text{cell}/\lambda$ (λ is the wavelength corresponding to $f_{\max}$) as the benchmark, the difference from the high-order method with $10\,\text{cell}/\lambda$ is in good agreement with it while less CPU time and memory requirement are needed. When a lower sampling density of $8\,\text{cell}/\lambda$ is involved, much less CPU time and memory
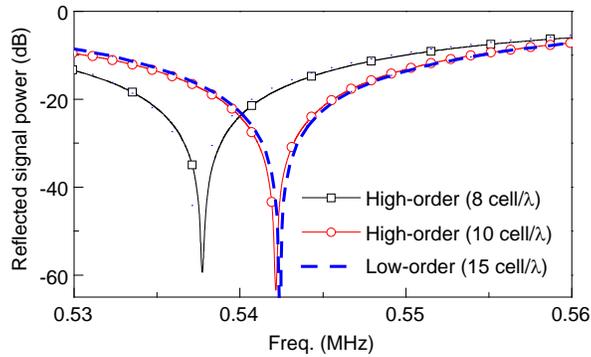
Figure 5. Reflected signal power calculated with high- and low-order WLP-FDTDs.

Table 3. Comparison between Different Methods.

Method	Meshing size	Memory (MB)	CPU time (s)	Difference (%)
High-order ($8\,\text{cell}/\lambda$)	160×32	5.15	64	0.87
High-order ($10\,\text{cell}/\lambda$)	200×40	7.23	97	0.037
Low-order ($15\,\text{cell}/\lambda$)	300×60	11.7	126	-

requirement are needed with the accepted numerical difference. The difference are calculated by the formula: $(P_{\min}^{H-O} - P_{\min}^{B-M})/P_{\min}^{B-M} \times 100\%$, where $P_{\min}^{H-O}$, $P_{\min}^{B-M}$ index the minimum reflected signal power for high order and the benchmark, respectively. The value of relative permeability is equal to 1. All calculations have been performed on an AMD Phenom II $\times 6$ 2.80 GHz machine with 8 GB RAM.

4. CONCLUSION

In this paper, with the fourth-order central difference in space domain, the numerical dispersion of high-order 2-D WLP-FDTD is analyzed. Its dispersion relation is associated with the propagation direction, sampling density in space domain and time-scale factor. Different from the conventional FDTD, the suitable selection of the time-scale factor leads to low numerical dispersion errors. Furthermore, compared with low-order WLP-FDTD, good dispersion characteristic can be observed with the low sampling density.

ACKNOWLEDGMENT

REFERENCES

1. Taflove, A. and S. C. Hagness, *Computational Electrodynamics: The Finite-difference Time-domain Method*, Artech House, Boston, MA, 2005.

2. Chung, Y. S., T. K. Sarkar, B. H. Jung, and M. Salazar-Palma, "An unconditionally stable scheme for the finite-difference time-domain method," *IEEE Trans. on Microwave Theory and Technique*, Vol. 51, No. 3, 697–704, 2003.

3. Duan, Y.-T., B. Chen, and Y. Yi, "Efficient implementation for the unconditionally stable 2-D WLP-FDTD method," *IEEE Microw. Wireless Compon. Lett.*, Vol. 19, No. 11, 677–679, 2007.

4. Duan, Y. T., B. Chen, D.-G. Fang, and B.-H. Zhou, "Efficient implementation for 3-D Laguerre-based finite-difference time-domain method," *IEEE Trans. on Microwave Theory and Technique*, Vol. 59, No. 1, 56–64, Jan. 2011

5. Chen, Z., Y. T. Duan, Y. R. Zhang, and Y. Yi, "A new efficient algorithm for the unconditionally stable 2-D WLP-FDTD method," *IEEE Trans. Antennas Propag.*, Vol. 61, No. 7, 3712–3720, Jul. 2013.

6. Chen, Z., Y. T. Duan, Y. R. Zhang, H.-L. Chen, and Y. Yi, "A new efficient algorithm for 3-D Laguerre-based finite-difference time-domain method," *IEEE Trans. Antennas Propag.*, Vol. 62, No. 4, 2158–2164, Apr. 2014.

7. He, G.-Q., W. Shao, X.-H. Wang, and B.-Z. Wang, "An efficient domain decomposition Laguerre-FDTD method for two-dimensional scattering problems," *IEEE Trans. Antennas Propag.*, Vol. 61, No. 5, 2639–2645, May 2013.

8. Alighanbari, A. and C. D. Sarris, "An unconditionally stable Laguerre-based S-MRTD time-domain scheme," *IEEE Antennas Wireless Propag. Lett.*, Vol. 5, 69–72, 2006.

9. Profy, F. and Z. Chen, "Efficient mixed-order FDTD using the Laguerre polynomials on non-uniform meshes," *IEEE/MTT-S International Microwave Symposium*, 1967–1970, Jun. 2007.

10. Chen, W.-J., W. Shao, J.-L. Li, and B.-Z. Wang, "Numerical dispersion analysis and key parameter selection in Laguerre-FDTD method," *IEEE Microw. Wireless Compon. Lett.*, Vol. 23, No. 12, 629–631, Dec. 2013.

11. Gustafsson, B., *High Order Difference Methods for Time Dependent PDE*, Springer, Berlin, Heidelberg, 2008

12. Pozar, D. M., *Microwave Engineering*, 4th edition, John Wiley, Hamilton, 2012.